nature physics

Article

https://doi.org/10.1038/s41567-026-03394-1

Quantification of elastic barriers to rearrangement in molecular glasses

Received: 25 November 2025

Accepted: 29 June 2026

Published online: 31 July 2026

Check for updates

Peng Luo[1,4] ✉, Zixuan Lin[1], Yixing Cao[1], Kritika Jha[1], Sarah E. Wolf[2], Shivajee Govind[1], Juliana I. Bonilla-Lugo[1], Richard B. Stephens[1,3] & Zahra Fakhraai[1] ✉

The glass transition is marked by a rapid increase in the barriers for molecular rearrangement, and this leads to the vitrification of supercooled liquids. Recent theories suggested that at low temperature, molecular rearrangements generate elastic stresses that dissipate through the surrounding material and add a non-local contribution to relaxation barriers. However, it is difficult to experimentally measure this elastic contribution. Here we measure the elastic barriers by investigating the transformation of vapour-deposited stable glasses, influenced by distant boundaries of varying elasticity. Rigid boundaries preserve bulk super-Arrhenius dynamics in which both relaxation times and barriers increase on supercooling. By contrast, distant soft boundaries facilitate fast Arrhenius relaxations—even below the glass transition temperature—by allowing faraway stress dissipation. As such, the constant soft-substrate barrier is attributed to local interactions, whereas the differences between barriers on soft and rigid boundaries arise from non-local elastic barriers. Our results show that the rapid dynamical slowdown and vitrification of supercooled liquids are governed by the emergence and growth of elastic barriers, and provide a direct experimental basis for elasticity-based descriptions of the glass transition.

The glass transition, where a supercooled liquid (SCL) abruptly falls out of equilibrium at the glass transition temperature (T_g), is accompanied by a rapid non-Arrhenius increase in structural relaxation time (τ_α). This means that the activation energies for structural relaxation grow rapidly within a small temperature range. The microscopic origin of this dramatic slowdown in dynamics remains an open question. Recent theories suggest that on supercooling, local rearrangements generate stress fields, which must be dissipated by a viscoelastic response from the dense surrounding medium[1–6], giving rise to additional barriers to molecular relaxation. These elasticity-induced barriers with their long-range effects add to the 'local' barriers, imposed by intermolecular interactions. It has been suggested that the 'non-local elastic' barriers, which grow with the decreasing compliance of the material on cooling, are critical in glass vitrification. However, distinguishing the influence of elasticity from that of other factors, such as growing cooperative rearrangements, to measure the size of non-local elastic barriers, remains a major experimental challenge.

The non-Arrhenius relaxation dynamics in SCLs are accompanied by a pronounced increase in the dynamic heterogeneity between neighbouring domains[7–9]. A key theoretical framework for understanding dynamic heterogeneity is kinetic facilitation (KF) in which local mobility is influenced and, thus, triggered by that of neighbouring regions[10,11]. KF is believed to be predominantly local, with a region's mobility influencing that of the nearest neighbours or within the range of intermolecular interaction potential[10,12,13]. However, recent computational studies suggest that elasticity can influence rearrangements over greater

[1]Department of Chemistry, University of Pennsylvania, Philadelphia, PA, USA. [2]Department of Chemistry, State University of New York Cortland, Cortland, NY, USA. [3]The Department of Physics and Astronomy, University of Pennsylvania, Philadelphia, PA, USA. [4]Present address: Institute of Physics, Chinese Academy of Sciences, Beijing, China. ✉e-mail: pengluo@iphy.ac.cn; fakhraai@sas.upenn.edu

distances, potentially mediating KF beyond local interactions[5,14,15]. In simulations of three-dimensional metallic glasses, mobile regions were observed to coexist with rigid elastic domains. The percolation of the elastic domains on decreasing temperature resulted in vitrification[16].

Although direct experimental measurements of elasticity-induced KF are not available to the best of our knowledge, it has been shown that the local T_g of polymer glasses in contact with low-modulus rubbery polymers is reduced as far as 200 nm away from the interface[17,18]. However, these effects have mostly been observed for high-molecular-weight polymers (M_w > 650 kg mol^{-1}), which have to be annealed to form a gradually varying interfacial layer, before the effects are apparent[17–19].

Stable glasses (SGs), which are prepared by physical vapour deposition (PVD)[20,21], offer a unique opportunity to probe local relaxation dynamics. On heating, SGs transform through kinetically facilitated transformation fronts[22–26]. By contrast, transformation can occur homogeneously throughout a liquid-quenched glass (LQG). The front transformation in SGs is governed by local relaxation dynamics at the advancing interface, with a driving force that is governed by the distance from equilibrium at the measurement temperature[25–28].

We have recently demonstrated that SG stability is affected up to ~170 nm away, when deposited on a soft substrate[29], providing indirect evidence for the importance of elasticity in relaxation dynamics. Here we study SG transformation kinetics on substrates with varying elasticity to directly measure the influence of elasticity on the size and the temperature dependence of barriers to rearrangement in molecular glasses. To eliminate direct interfacial effects, we designed a 'buried' SG/LQG interface in bilayer films of *N*,*N*′-bis(3-methylphenyl)-*N*,*N*′-diphenylbenzidine (TPD), with 50-nm-thick LQG layers separating 130-nm-thick SG layers from substrates of varying elasticity. To measure the transformation kinetics of this interface, we used spectroscopic ellipsometry (SE) to monitor the evolution of the SG/LQG interface position during isothermal annealing. We demonstrate that a 'soft boundary', an interface with a material of low elastic modulus, strongly enhances relaxation dynamics more than 100 nm away, far exceeding the range of TPD's local van der Waals intermolecular interactions. By performing experiments over a broad temperature range and prolonged timescales, we observe bulk-like non-Arrhenius dynamics (growing relaxation barriers) in the presence of a rigid boundary, whereas we see Arrhenius dynamics (nearly constant barriers) with a soft boundary. Using these data, we estimate the contribution of the non-local elastic barriers to the relaxation dynamics and show that it increases on cooling. The elastic barrier component exceeds that of local interactions just below T_g. These findings identify elasticity as a key origin for non-Arrhenius dynamics in molecular glasses and highlight its role in glass vitrification.

Bilayer geometry design to investigate how elasticity affects KF

We hypothesize that the elastic nature of the boundary, even if it is located far away, can kinetically facilitate the relaxation dynamics in glasses, by allowing stress dissipation through the boundary (Fig. 1). To probe this elasticity-induced KF, we prepared a transforming interface with invariant local relaxations. SG (130 nm)/LQG (50 nm) bilayer films of TPD (Young's modulus of $E \approx 7$ GPa (ref. 29)) were prepared through PVD. These films were deposited on three substrates with different elastic moduli: bare silicon ($E \approx 75$ GPa (ref. 18), denoted as rigid), a silicon wafer covered with a 5-nm-thick polydimethylsiloxane (PDMS) rubber film cured at 383 K ($E \approx 4.8$ MPa, semi-soft) and another with the 5-nm PDMS cured at 295 K ($E \approx 3.9$ MPa, soft)[29]. Sample preparation details can be found in Methods. The measured T_g values of the LQG layer on both rigid and soft substrates were identical ($T_g = 329 \pm 1$ K at 10 K min^{-1}; Extended Data Fig. 1a,b), and similar to the bulk T_g (331 ± 1 K (ref. 29)).

Despite being separated from the substrate by a 50-nm LQG buffer layer, the SG layers deposited on soft substrates remain more stable and more isotropically oriented than those on rigid substrates

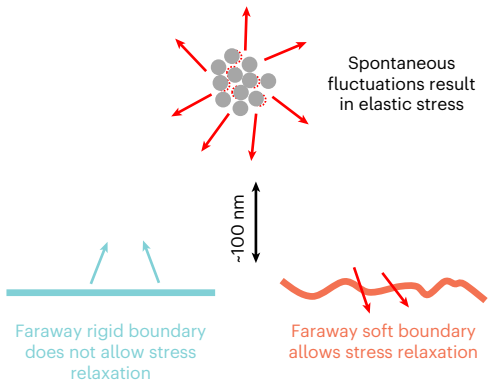


Fig. 1 | Schematics illustrating the influence of boundary elasticity on faraway relaxation dynamics. Spontaneous molecular relaxations in a deeply SCL or glass can generate elastic stresses that propagate over a long distance before dissipation. A rigid boundary prevents stress dissipation; the barriers to relaxation are bulk-like. With a soft boundary, the propagating elastic stresses can dissipate through the interface, thereby reducing the elastic barriers to near-zero; the relaxation barriers are the same as the local barriers at high temperatures.

(Extended Data Fig. 1c–h). Their fictive temperatures $T_{f,SG}$, defined as the temperature at which the glass has the same thermodynamic state as the SCL[21], are 270 ± 2, 282 ± 1 and 286 ± 2 K on soft, semi-soft and rigid substrates, respectively, consistent with those of single-layer SGs deposited directly on the corresponding substrates. This provides strong evidence that the effect of substrate softness propagates over distances far exceeding the range of direct molecular interactions. We also note that although in most PVD systems, a lower fictive temperature (higher stability) typically results in slower transformation fronts[22,30], our data show the opposite trend in these layers, as discussed further below. Moreover, prior work has shown that $T_{f,SG}$ does not affect the activation energy of the transformation[30]. Therefore, we do not expect these differences in $T_{f,SG}$ to affect the measured activation energies in this study. As such, the local interactions and relaxation barriers at the buried SG/LQG interface are reasonably similar across substrates, whereas the non-local elastic barriers are systematically tuned, allowing us to compare and evaluate barriers arising from longer-range effects.

Figure 2 schematically illustrates the evolution of the buried SG/LQG interface on isothermal annealing, used to explore KF. At annealing temperatures $T_{iso} > T_g$, the layer directly on the substrate quickly transforms into the SCL state and does not further evolve, whereas the upper SG layer transforms more slowly through a growth front. This results in an upward shift of the buried SG/transformed SCL interface position (denoted as z_b in Fig. 2b), as measured by SE. When $T_{f,SG} < T_{iso} < T_g$, in addition to the SG transformation (Fig. 2a, blue-violet arrows), the LQG layer is expected to undergo physical aging (turquoise arrows), which should reduce its specific volume, creating a competing downward shift of z_b (Fig. 2c). The instantaneous change in z_b is calculated as

$$dz_b/dt = v_{gr,b} - v_{ag}, \quad (1)$$

where $v_{gr,b}$ is the growth front velocity of SG and v_{ag} is the rate of change of the LQG layer thickness due to physical aging (that is, the evolution of the LQG towards the equilibrium SCL state). $v_{gr,b}$ depends on the driving force to reach equilibrium, determined by the interplay between the SG stability and the local relaxation dynamics of the transformed SCL at T_{iso} (refs. 30,31). As such, its dependence on T_{iso} is governed by the temperature dependence of τ_α at the SG/LQG interface[25–28,32]. In other words, a shorter τ_α results in a larger $v_{gr,b}$ for a glass with certain stability. We note that the free surface also has a transformation growth front[30]. The SG layer thickness is chosen such that this surface interface

https://doi.org/10.1038/s41567-026-03394-1

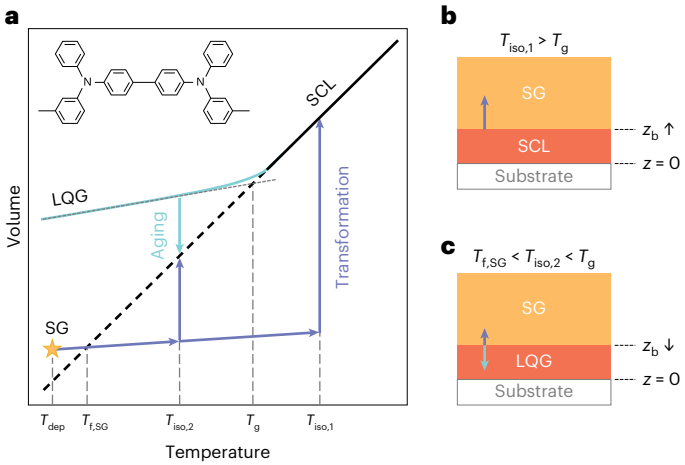


Fig. 2 | Schemes illustrating physical aging and transformation at the buried SG/LQG interface in bilayer films. a, Schematic showing where certain states exist with respect to volume and temperature, with the molecular structure of TPD (inset). **b**, During isothermal annealing at $T_{iso,1} > T_g$, the layer on the substrate is at equilibrium (SCL), whereas the upper SG layer progressively transforms into SCL (blue-violet arrows in **a** and **b**) at the SG/SCL interface. This addition to the SCL layer results in an upward shift of z_b. **c**, At $T_{f,SG} < T_{iso,2} < T_g$, the LQG layer on the substrate ages towards the corresponding equilibrium SCL state (turquoise arrows in **a** and **b**), which has a lower volume. The upper SG layer also transforms towards the same SCL state (blue-violet arrows in **a** and **b**), but at a much slower rate, due to its stability. Increasing density of the aging LQG dominates and results in a downward shift of z_b.

does not influence the transformation kinetics at the buried SG/LQG interface within the experimental window.

Facilitation of relaxation dynamics by soft substrate

Using SE, we are able to directly probe the evolution of z_b during isothermal annealing at various temperatures (Fig. 3). The average upward shift rate of the buried interface, $<dz_b/dt>$, was obtained from linear fits to the z_b profiles. At $1.01T_g$ (Fig. 3a), $<dz_b/dt>$ is substantially larger on the soft substrate than on the rigid substrate. Independent trials at $1.04T_g$ (Extended Data Fig. 2a) indicate that this enhancement is well beyond experimental error ($(5.0 \pm 0.2) \times 10^{-2}$ nm s^{-1} on the soft substrate versus $(2.2 \pm 0.2) \times 10^{-2}$ nm s^{-1} on the rigid substrate). The difference in the transformation rate persists even when the buried interface is placed 70 nm away from the substrate (Extended Data Fig. 2a), showing its long-range influence. This effect is observed down to $0.997T_g$ (Fig. 3b), where the difference in $<dz_b/dt>$ becomes more pronounced, by a factor of 10 (3.9×10^{-5} nm s^{-1} on the soft substrate versus 3.8×10^{-6} nm s^{-1} on the rigid substrate). This enhancement in the transformation rate on the soft substrate is remarkable because its SG layer has a lower $T_{f,SG}$ than the SG layer on the rigid substrate, which can indicate the relatively enhanced stability of the soft-substrate sample.

At $0.98T_g$ (Fig. 3c), z_b of the samples on rigid substrates exhibits a continuous downward shift within the experimental time window of ~9 days, meaning that the rate of physical aging is faster than that of SG transformation through the growth front ($v_{ag} > v_{gr,b}$, equation (1)). This is the expected behaviour of a bulk glass because the LQG is less stable than the SG, and should, as such, evolve more rapidly towards equilibrium. As a result, as schematically shown in Fig. 2, a downward shift of the interface is observed. The normalized $<dz_b/dt>$ values are also comparable with the previously reported average aging rates of bulk LQG films[33] (Extended Data Fig. 3 and Extended Data Table 1), indicating that the SG transformation is now much slower than can be experimentally measured. On a semi-soft substrate also at $0.98T_g$, the two competing processes appear to have the exact same rate, maintaining the interface at the same location for $>6 \times 10^5$ s (~7 days). On the soft substrate, z_b still moves upwards ($(5.2 \pm 0.9) \times 10^{-6}$ nm s^{-1}, the average value for the two independent trials), indicating that the SG transformation remains fast probably because the LQG has already reached equilibrium due to enhanced dynamics. The combined data (Fig. 3 and Extended Data Fig. 2) reveal that a soft boundary a distance away dramatically facilitates the relaxation dynamics at the buried SG/LQG interface. In particular, the constant rate of transformation at all temperatures means that this effect persists up to a distance of at least 100 nm away. The observation is limited at low temperatures, because it requires prohibitively long observation times.

Influence of boundary elasticity on the temperature dependence of faraway relaxation dynamics

The dynamics can be further characterized by considering the average growth front velocity, $<v_{gr,b}>$, which can be calculated using equation (1) and $<dz_b/dt>$ obtained from the SE data; $<v_{ag}>$ was estimated using the aging studies in ref. 33 (Methods). However, as shown in Extended Data Fig. 3, $<dz_b/dt>$ and $<v_{gr,b}>$ have similar values, due to the negligible role of aging at the studied temperatures. Figure 4a compares the temperature dependence of $<v_{gr,b}>$ for samples on soft and rigid substrates with the bulk τ_α of TPD, obtained from dielectric relaxation measurements in ref. 30. The temperature dependence of $<v_{gr,b}>$ for glass on the rigid substrate closely follows that of the bulk τ_α, whereas $<v_{gr,b}>$ on the soft substrate is faster at all temperatures, with the difference becoming more pronounced with decreasing temperature. At T_g, the transformation is about one decade faster on soft substrates. This difference already far exceeds the experimental uncertainty. A conservative Arrhenius extrapolation of $<v_{gr,b}>$ to the deposition temperature, $T_{dep} = 264$ K, predicts at least a 10^5-fold higher transformation rate and, thus, a correspondingly shorter τ_α, on the soft substrate (Extended Data Fig. 4a). This difference explains our previous observation that denser and more stable glasses can be produced on soft substrates, for which we had previously estimated a 10^5–10^7 enhancement in the rate of surface-mediated equilibration[29].

For various systems (including TPD) with SGs on rigid substrates, the transformation front velocities initiated at the free surface (v_{gr}) typically show a weaker dependence on the transformation temperature than bulk τ_α of the transformed SCL, usually following ($v_{gr} \propto \tau_\alpha^{-\gamma}$) with $\gamma \simeq 0.7$–0.8 (refs. 30,34,35). For our bilayer samples on rigid substrates (Extended Data Fig. 5a), the front velocity at the buried interface is roughly proportional to the rate of structural relaxations ($<v_{gr,b}> \propto \tau_\alpha^{-1}$). This indicates that the transformation velocity at a buried interface more closely represents bulk relaxation dynamics than the dynamics of transformation fronts at the free surface. Interestingly, for bilayer glass on soft substrates, the power-law dependence resembles that of the free surface ($<v_{gr,b}> \propto \tau_\alpha^{-0.64 \pm 0.05}$; Extended Data Fig. 5a), matching the results for single-layer TPD at $T_{dep} = 260$ K and $T_{dep} = 280$ K (ref. 30; Extended Data Fig. 5b). This is an indirect indication that the free surface can also act as a soft boundary, providing a potential explanation for the weak temperature dependence of growth front velocities, independent of glass stability[30,34,35]. This possibility merits future in-depth investigation.

Temperature dependence of relaxation barriers

The contrasting behaviour in the dynamics of bilayer glasses on different substrates primarily arises from the growing divergences of their relaxation barriers, as the temperature is decreased. As mentioned above, $<v_{gr,b}> \propto \tau_\alpha^{-1}$ for the bilayer on rigid substrates; therefore, the temperature dependence of the activation energy (ΔE_{rigid}) can be obtained from the previously measured bulk τ_α (ref. 30). The activation energy of the bulk, ΔE_{bulk}, can be obtained from τ_α (slope of the solid black line in Fig. 4a), which shows an increase from ~443 kJ mol^{-1} at $1.06T_g$ to ~841 kJ mol^{-1} at $0.97T_g$. On soft substrates, the bilayer's $<v_{gr,b}>$

https://doi.org/10.1038/s41567-026-03394-1

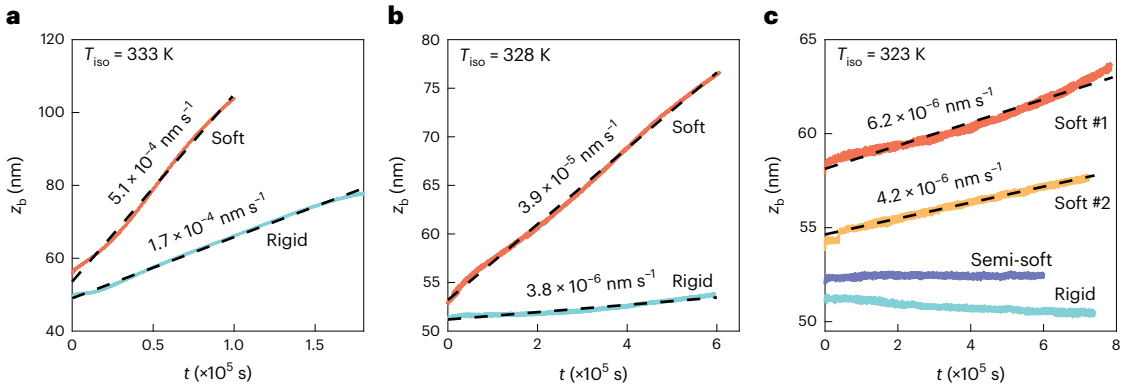


Fig. 3 | Transformation kinetics at the buried SG/LQG interface in bilayer films. **a**–**c**, z_b versus time (t) during isothermal annealing at various T_{iso} values: 333 K ($1.01T_g$; **a**); 328 K ($0.997T_g$; **b**); 323 K ($0.98T_g$; **c**). The bilayer glasses were prepared on soft (two independent trials at T_{iso} = 323 K), semi-soft and rigid substrates. Dashed lines show linear fits, from which the $<dz_b/dt>$ values (the slopes, as labelled above each line) were calculated.

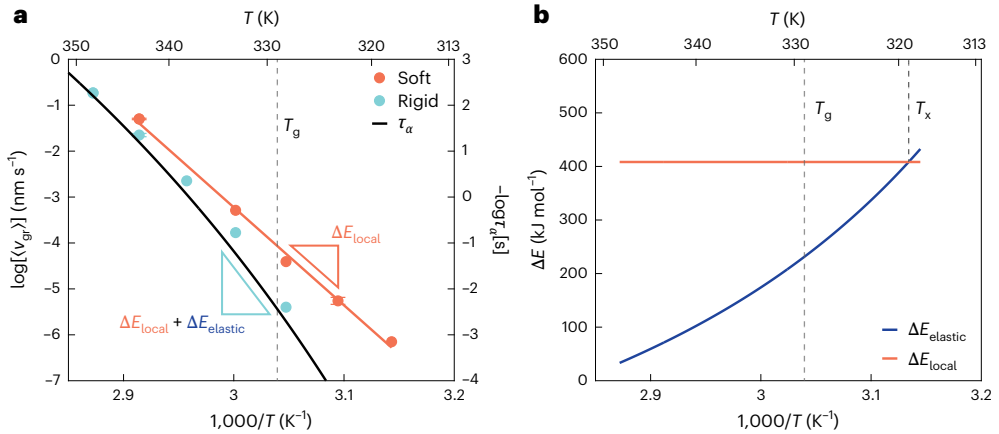


Fig. 4 | Temperature dependence of relaxation dynamics and barriers. **a**, Arrhenius plot of $<v_{gr,b}>$ (left axis) for bilayer glass on soft (red) and rigid (turquoise) substrates versus inverse temperature (1,000/T, corresponding temperature values shown on top). Data with error bars are presented as mean values ± standard error of the mean for three independent experiments. Data are compared with τ_α of bulk TPD (black line, right axis), represented by a Vogel–Fulcher–Tammann (VFT) fit, $\tau_\alpha = \tau_0 \exp\left(\frac{B}{T-T_0}\right)$, with $\tau_0 = 10^{-19.2}$ s, B = 3,493 K (29.0 kJ mol^{-1}) and T_0 = 258.9 K. Arrhenius fit to the $<v_{gr,b}>$ data on soft substrates (solid red line) yields an activation energy of ΔE_{soft} = 408 ± 15 kJ mol^{-1}. **b**, Comparison between the overall local barrier (red, $\Delta E_{local} \simeq \Delta E_{soft}$, as schematically indicated in **a**) and overall non-local elastic barrier (blue, $\Delta E_{elastic} \simeq \Delta E_{rigid} - \Delta E_{soft}$, as schematically indicated in **a**) as a function of inverse temperature (1,000/T, corresponding temperature values shown on top). The dashed lines denote T_g = 329 K and T_x = 319 ± 1 K (where $\Delta E_{elastic} \simeq \Delta E_{local}$). τ_α data in panel **a** adapted with permission from ref. 30, AIP.

exhibits Arrhenius behaviour with a constant activation energy with ΔE_{soft} = 408 ± 15 kJ mol^{-1}, over the experimental window, spanning almost eight decades in τ_α and down to $0.97T_g$.

Given the similarity between ΔE_{rigid} and ΔE_{bulk}, we can assume that similar to ΔE_{bulk}, ΔE_{rigid} is composed of two components: $\Delta E_{rigid} = \Delta E_{bulk} = \Delta E_{local} + \Delta E_{elastic}$ (refs. 2,36), where ΔE_{local} is the relaxation barrier component due to local means and $\Delta E_{elastic}$ is the barrier component due to non-local and elastic factors. To estimate ΔE_{local}, we note that the barrier for samples on soft substrates (ΔE_{soft}) is temperature-independent and that $\Delta E_{soft} < \Delta E_{rigid}$ in the experimental window. As such, we can assume that the elastic barrier is negligible due to dissipation through the soft substrate: $\Delta E_{local} \simeq \Delta E_{soft}$. Thus, we can evaluate the activation energy due to elasticity (the overall elastic barrier) with $\Delta E_{elastic} = \Delta E_{bulk} - \Delta E_{soft}$. Figure 4b compares $\Delta E_{elastic}$ with ΔE_{local}. At high temperatures, the elastic barrier is negligible ($\Delta E_{elastic}$ = 35 kJ mol^{-1} at $1.06T_g$), but it dramatically grows on cooling. The elastic barrier exceeds ΔE_{local} at a crossover temperature just below T_g ($T_x = 0.97T_g$).

We note that previous theoretical work had predicted T_x to be well above T_g (ref. 36). One possible explanation is that ΔE_{soft} is only an upper-bound value for ΔE_{local}. However, to match the high crossover temperatures predicted in simulations, ΔE_{local} would have to be half the measured value here. This is unlikely, given that $\Delta E_{bulk} \simeq \Delta E_{soft}$ even at $1.11T_g$ (Extended Data Fig. 4b), the highest temperature at which τ_α was measured[30]. Since $\Delta E_{bulk} \geq \Delta E_{local}$ at all temperatures, any temperature dependence of ΔE_{local} must be negligible in our experimental window, corroborating the assumption that $\Delta E_{soft} \simeq \Delta E_{local}$. Another possibility for this discrepancy is that glass simulations are often performed in small boxes with periodic boundaries and are quenched at much higher cooling rates. As such, it is likely that their estimated crossover temperatures are higher than those in experiments.

Effect of elastic barrier on vitrification

Figure 1 schematically shows how a local rearrangement may result in long-range elastic stresses, which may be dissipated differently at a rigid (reflective) versus soft (dissipative) boundary a far distance away. Our data demonstrate that without invoking any specific local dynamical correlations, these differences can result in dramatically different relaxation barriers, at least 100 nm away from an interface. It is remarkable that the elastic facilitation of a soft substrate results in Arrhenius temperature dependence, indicating that growing or

percolating elasticity may be the main origin of non-Arrhenius relaxation dynamics[1,3–6,16]. This is consistent with recent inelastic neutron scattering experiments, which suggested a coupling between the development of shear elasticity and the emergence of non-Arrhenius relaxations[37]. Elasticity-mediated KF may also explain previous observations that under mechanical deformation, relaxation dynamics become more homogeneous[38]; in other words, the origin of non-exponential relaxation decay may be the heterogeneity of elastic barriers, as opposed to local barriers. Our data can also potentially explain why SGs, equilibrated at $0.85T_g$, have nucleation sites that are >1 µm away from each other[26,32]. This is probably the length scale at which individual relaxation events that rely on elastic dissipation become reasonably uncorrelated[32,39].

We note that our prediction of T_x solely relies on the slope of the Arrhenius curves. As such, it is remarkable that the estimated value of T_x is so close to T_g, obtained by dilatometry or calorimetry experiments, despite the uncertainties involved. This is a strong indication that an elastic percolation[6] may indeed be the primary origin of vitrification, as T_g is approached from above. However, it is also important to note that T_g, a quantity determined using the average relaxation dynamics of the SCL, will not clearly show these elasticity effects because these effects only become pronounced at low temperatures, only affecting the lower onset of vitrification, as opposed to the average. This can explain why the T_g of the 50-nm LQG layers is only marginally affected by the substrate elasticity.

TPD is a fragile liquid, with non-Arrhenius temperature dependence[30,40]. Its viscosity dramatically decreases with increasing temperature, explaining why its elastic barriers would quickly vanish above T_g (Fig. 4b). In strong liquids, we expect elastic barriers to remain high—well above T_g—contributing to their higher viscosity at the same reduced temperatures[40]. This accounts for why their temperature-dependent relaxation times would remain Arrhenius; both local and elastic barriers are weakly temperature dependent. Strong liquids often exhibit a narrower distribution of relaxation times than fragile liquids[41], which may similarly be explained by the weaker temperature dependence of both barriers.

In summary, this work experimentally demonstrates the strong contribution of elastic dissipation to the relaxation barriers in molecular glasses. The data suggest that the contribution of the non-local elastic barriers increases rapidly at low temperatures, thereby playing a key role in the rapid non-Arrhenius slowdown of relaxation dynamics and subsequent vitrification. Dissipation of elastic stresses enabled by a soft boundary a far distance away can mitigate this percolating effect, thereby facilitating glass equilibration, even well below T_g. This work demonstrates that the addition of thin, rubbery films as soft substrates can be used as an approach to prevent glass vitrification at a far distance away, and produce dramatically better equilibrated glasses at low temperatures, particularly through PVD. In addition to their potential industrial applications, the estimated elasticity-induced barriers and the resulting insights into how glass relaxation is influenced by boundaries well below T_g can help improve theoretical models for the glass transition.

Online content

Any methods, additional references, Nature Portfolio reporting summaries, source data, extended data, supplementary information, acknowledgements, peer review information; details of author contributions and competing interests; and statements of data and code availability are available at https://doi.org/10.1038/s41567-026-03394-1.

References

1. Ghanekarade, A., Phan, A. D., Schweizer, K. S. & Simmons, D. S. Signature of collective elastic glass physics in surface-induced long-range tails in dynamical gradients. *Nat. Phys.* **19**, 800–806 (2023).
2. Mirigian, S. & Schweizer, K. S. Elastically cooperative activated barrier hopping theory of relaxation in viscous fluids. I. General formulation and application to hard sphere fluids. *J. Chem. Phys.* **140**, 194506 (2014).
3. Phan, A. D. & Schweizer, K. S. Effect of the nature of the solid substrate on spatially heterogeneous activated dynamics in glass forming supported films. *J. Chem. Phys.* **160**, 074902 (2024).
4. Lemaître, A. Structural relaxation is a scale-free process. *Phys. Rev. Lett.* **113**, 245702 (2014).
5. Hasyim, M. R. & Mandadapu, K. K. Emergent facilitation and glassy dynamics in supercooled liquids. *Proc. Natl Acad. Sci. USA* **121**, e2322592121 (2024).
6. Dyre, J. C. & Olsen, N. B. Landscape equivalent of the shoving model. *Phys. Rev. E* **69**, 042501 (2004).
7. Ediger, M. D. Spatially heterogeneous dynamics in supercooled liquids. *Annu. Rev. Phys. Chem.* **51**, 99–128 (2000).
8. Mandel, N. L., Rehman, T. & Kaufman, L. J. Manifestations of static and dynamic heterogeneity in single molecule translational measurements in glassy systems. *J. Chem. Phys.* **157**, 184506 (2022).
9. Mauro, J. C., Uzun, S. S., Bras, W. & Sen, S. Nonmonotonic evolution of density fluctuations during glass relaxation. *Phys. Rev. Lett.* **102**, 155506 (2009).
10. Keys, A. S., Hedges, L. O., Garrahan, J. P., Glotzer, S. C. & Chandler, D. Excitations are localized and relaxation is hierarchical in glass-forming liquids. *Phys. Rev. X* **1**, 021013 (2011).
11. Butler, S. & Harrowell, P. The origin of glassy dynamics in the 2D facilitated kinetic Ising model. *J. Chem. Phys.* **95**, 4454–4465 (1991).
12. Chacko, R. N. et al. Dynamical facilitation governs the equilibration dynamics of glasses. *Phys. Rev. X* **14**, 031012 (2024).
13. Candelier, R. et al. Spatiotemporal hierarchy of relaxation events, dynamical heterogeneities, and structural reorganization in a supercooled liquid. *Phys. Rev. Lett.* **105**, 135702 (2010).
14. Chacko, R. N. et al. Elastoplasticity mediates dynamical heterogeneity below the mode coupling temperature. *Phys. Rev. Lett.* **127**, 048002 (2021).
15. Ozawa, M. & Biroli, G. Elasticity, facilitation, and dynamic heterogeneity in glass-forming liquids. *Phys. Rev. Lett.* **130**, 138201 (2023).
16. Gao, L., Yu, H.-B., Schrøder, T. B. & Dyre, J. C. Unified percolation scenario for the α and β processes in simple glass formers. *Nat. Phys.* **21**, 471–479 (2025).
17. Baglay, R. R. & Roth, C. B. Local glass transition temperature $T_g(z)$ of polystyrene next to different polymers: hard vs. soft confinement. *J. Chem. Phys.* **146**, 203307 (2017).
18. Gagnon, Y. J. & Roth, C. B. Local glass transition temperature $T_g(z)$ within polystyrene is strongly impacted by the modulus of the neighboring pdms domain. *ACS Macro Lett.* **9**, 1625–1631 (2020).
19. Gagnon, Y. J., Burton, J. C. & Roth, C. B. Development of broad modulus profile upon polymer–polymer interface formation between immiscible glassy–rubbery domains. *Proc. Natl Acad. Sci. USA* **121**, e2312533120 (2024).
20. Swallen, S. F. et al. Organic glasses with exceptional thermodynamic and kinetic stability. *Science* **315**, 353–356 (2007).
21. Luo, P. & Fakhraai, Z. Surface-mediated formation of stable glasses. *Annu. Rev. Phys. Chem.* **74**, 361–389 (2023).
22. Rodríguez-Tinoco, C., Gonzalez-Silveira, M., Ràfols-Ribé, J., Lopeandía, A. F. & Rodríguez-Viejo, J. Transformation kinetics of vapor-deposited thin film organic glasses: the role of stability and molecular packing anisotropy. *Phys. Chem. Chem. Phys.* **17**, 31195–31201 (2015).
23. Sepúlveda, A., Swallen, S. F. & Ediger, M. D. Manipulating the properties of stable organic glasses using kinetic facilitation. *J. Chem. Phys.* **138**, 12A517 (2013).
24. Flenner, E., Berthier, L., Charbonneau, P. & Fullerton, C. J. Front-mediated melting of isotropic ultrastable glasses. *Phys. Rev. Lett.* **123**, 175501 (2019).

25. Vila-Costa, A., Gonzalez-Silveira, M., Rodríguez-Tinoco, C., Rodríguez-López, M. & Rodriguez-Viejo, J. Emergence of equilibrated liquid regions within the glass. *Nat. Phys.* **19**, 114–119 (2023).
26. Ruiz-Ruiz, M. et al. Real-time microscopy of the relaxation of a glass. *Nat. Phys.* **19**, 1509–1515 (2023).
27. Herrero, C., Scalliet, C., Ediger, M. & Berthier, L. Two-step devitrification of ultrastable glasses. *Proc. Natl Acad. Sci. USA* **120**, e2220824120 (2023).
28. Herrero, C., Ediger, M. D. & Berthier, L. Front propagation in ultrastable glasses is dynamically heterogeneous. *J. Chem. Phys.* **159**, 114504 (2023).
29. Luo, P. et al. High-density stable glasses formed on soft substrates. *Nat. Mater.* **23**, 688–694 (2024).
30. Walters, D. M., Richert, R. & Ediger, M. D. Thermal stability of vapor-deposited stable glasses of an organic semiconductor. *J. Chem. Phys.* **142**, 134504 (2015).
31. Rodríguez-Tinoco, C. et al. Surface-bulk interplay in vapor-deposited glasses: crossover length and the origin of front transformation. *Phys. Rev. Lett.* **123**, 155501 (2019).
32. Vila-Costa, A. et al. Nucleation and growth of the supercooled liquid phase control glass transition in bulk ultrastable glasses. *Phys. Rev. Lett.* **124**, 076002 (2020).
33. Cheng, S. et al. Physical aging of glasses of an organic semiconductor. *J. Mater. Chem. C* **13**, 13214–13223 (2025).
34. Rodríguez-Tinoco, C. et al. Evaluation of growth front velocity in ultrastable glasses of indomethacin over a wide temperature interval. *J. Phys. Chem. B* **118**, 10795–10801 (2014).
35. Sepúlveda, A., Tylinski, M., Guiseppi-Elie, A., Richert, R. & Ediger, M. Role of fragility in the formation of highly stable organic glasses. *Phys. Rev. Lett.* **113**, 045901 (2014).
36. Mirigian, S. & Schweizer, K. S. Elastically cooperative activated barrier hopping theory of relaxation in viscous fluids. II. *Thermal liquids. J. Chem. Phys.* **140**, 194507 (2014).
37. Luo, P. et al. Correlation between fast relaxation, shear phonon propagation, and dynamic heterogeneity in glass-forming liquids. *J. Chem. Phys.* **16**, 12386–12392 (2025).
38. Lee, H.-N., Paeng, K., Swallen, S. F. & Ediger, M. Direct measurement of molecular mobility in actively deformed polymer glasses. *Science* **323**, 231–234 (2009).
39. Dyre, J. C. Solid-that-flows picture of glass-forming liquids. *J. Phys. Chem. Lett.* **15**, 1603–1617 (2024).
40. Angell, C. A. Formation of glasses from liquids and biopolymers. *Science* **267**, 1924–1935 (1995).
41. Böhmer, R., Ngai, K. L., Angell, C. A. & Plazek, D. J. Nonexponential relaxations in strong and fragile glass formers. *J. Chem. Phys.* **99**, 4201–4209 (1993).

Publisher's note Springer Nature remains neutral with regard to jurisdictional claims in published maps and institutional affiliations.

Open Access This article is licensed under a Creative Commons Attribution-NonCommercial-NoDerivatives 4.0 International License, which permits any non-commercial use, sharing, distribution and reproduction in any medium or format, as long as you give appropriate credit to the original author(s) and the source, provide a link to the Creative Commons licence, and indicate if you modified the licensed material. You do not have permission under this licence to share adapted material derived from this article or parts of it. The images or other third party material in this article are included in the article's Creative Commons licence, unless indicated otherwise in a credit line to the material. If material is not included in the article's Creative Commons licence and your intended use is not permitted by statutory regulation or exceeds the permitted use, you will need to obtain permission directly from the copyright holder. To view a copy of this licence, visit http://creativecommons.org/licenses/by-nc-nd/4.0/.

© The Author(s) 2026

Methods

Sample preparation

PDMS substrate preparation. Thin-film PDMS substrates were made from SYLGARD 184 silicone elastomer kits (Dow Corning). The base and curing agents were mixed at a mass ratio of 10:1 and dissolved in toluene to prepare a stock solution of 10-wt% PDMS. The solution was shaken and ultrasonicated for 10 min for better dissolution and mixing. Diluted PDMS solutions with concentrations of 0.2 wt% were prepared from the stock solution and spun-cast on silicon wafers (<100> oriented, Virginia Semiconductor) at a rotating speed of 5,000 rpm, producing films with thicknesses of 5 ± 1 nm. The spun-cast PDMS films were subsequently cured under a vacuum at two different temperatures to make films with different elastic moduli. The films cured at room temperature (295 K) for 24 h have a modulus $E \approx 3.9$ MPa (denoted as soft), and those cured at 383 K for 1 h have $E \approx 4.8$ MPa (denoted as semi-soft), as reported in our recent work[29]. The potential effect of uncrosslinked PDMS and other free small molecules on the data was investigated by performing control experiments on cured PDMS films washed in toluene, as detailed in our previous work[29]. No difference was seen between the as-prepared and washed substrates in the results of the current work.

TPD film preparation. TPD was purchased from Sigma-Aldrich (purity, >99%) and used without further purification. PVD of TPD was carried out in a custom-designed ultrahigh-vacuum chamber, with a base pressure of ~10^{-7} torr, as described in our previous publication[29]. The distance between the deposition source and the temperature-controlled substrates was approximately 25 cm. The deposition rate was $R_{dep} = 2 \pm 0.2$ Å s^{-1}, monitored using a quartz crystal microbalance (Inficon STM-2 USB thin-film rate/thickness monitor) placed near the substrate stage. A shutter between the TPD source and the substrate was opened to start deposition after R_{dep} stabilized at the target value, and it was closed once the target film thickness was reached. The 180-nm-thick SG films were prepared by deposition at $T_{dep} = 264$ K. To prepare bilayer films, a 50-nm-thick SG layer was deposited at $T_{dep} = 264$ K, which was subsequently heated in situ to 343 K and annealed for 10 min to fully transform it into SCL. After the transformation, the sample was cooled back to 264 K, creating the LQG layer. Another 130-nm-thick SG layer was deposited on the 50-nm-thick LQG layer. Control experiments show that under these annealing conditions, the SG is fully transformed without dewetting, and all substrates and films had surface roughness of <2 nm (Extended Data Fig. 6).

SE characterization

SE measurements. Thin-film characterization and in situ experiments were performed on a J.A. Woollam M-2000V ellipsometer equipped with a Linkam stage (THMS600) for temperature control. A thin layer of high-temperature vacuum grease (Apiezon PFPE 501) was applied to ensure good thermal contact between the substrate and the stage. The ellipsometric angles Ψ (amplitude change) and Δ (phase change) were collected in the spectral wavelength range of 370 nm < λ < 1,700 nm. To improve accuracy and eliminate systematic error from polarizers, zone-averaged measurements were performed, in which the SE data were averaged based on two measurements acquired with the polarizer rotated by 90°.

The 5-nm-thick and 13-nm-thick PDMS films and the as-prepared and fully transformed TPD glass films and bilayers were characterized at 298 K by variable-angle spectroscopic ellipsometry (VASE) measurements, using incident angles from 55° to 75° (at 5° increment each), with an acquisition time of 20 s each.

For in situ dilatometry or isothermal experiments on bilayer films, the incident angle was fixed at 70°, and the data were collected with zone averaging at 2–30-s intervals depending on the duration of the experiment. When performing in situ isothermal annealing, each sample was heated to the target temperature (303–348 K) at a heating rate of 60 K min^{-1}. After the isothermal annealing experiments were concluded, the sample was heated to 353 K for full transformation of the entire film, followed by cooling at 10 K min^{-1} to 298 K.

SE data modelling. CompleteEASE software (v.6.66) was used for modelling the SE data. To avoid strong absorbance effects of TPD at wavelengths of λ < 400 nm (ref. 29), SE fitting for TPD films and bilayers was restricted to wavelengths from 550 to 1,700 nm. To obtain the temperature-dependent values of the optical properties of the PDMS substrates, 13-nm-thick PDMS films were characterized with this VASE measurement at constant temperatures (from 298 to 393 K, every 5-K interval), on both heating and cooling. The VASE data for PDMS films were fitted within the wavelength range of 370 to 1,700 nm. The results were reported in our previous work[29] and are reproduced here in Extended Data Fig. 7 for ease of reference.

To obtain the optical properties for LQG films, measurements were performed on fully transformed TPD films, and the data were modelled using a four-layer model: the silicon substrate, a 1.0-nm-thick native oxide, PDMS and an isotropic Cauchy film ($n = A + \frac{B}{\lambda^2}$, where n is the refractive index and A and B are constants) for TPD. With all other parameters known, A, B and the film thickness h_{film} were used as fitting parameters. A and B were then used as known parameters for the LQG layer when modelling bilayer films, without further fitting. Temperature-dependent ellipsometry data for the silicon substrate, available in the CompleteEASE library, were directly used in the modelling.

The optical properties of bilayer films on PDMS substrates were modelled using a five-layer model, including (from bottom to top) the silicon substrate, native silicon oxide layer, an isotropic Cauchy layer for PDMS, another isotropic Cauchy layer for LQG and an anisotropic (birefringent) Cauchy layer for SG, described as

$$n_{xy} = A_{xy} + \frac{B}{\lambda^2} \tag{2}$$

$$n_z = A_z + \frac{B}{\lambda^2} \tag{3}$$

where n_{xy} and n_z are the in-plane and out-of-plane refractive indices, respectively, and A_{xy}, A_z and B are Cauchy fit parameters. With all other parameters known, only A_{xy}, A_z, B and h_{SG} for the SG layer, along with h_{LQG} for the LQG layer, were used as fitting parameters.

For modelling the in situ SE data collected during isothermal annealing, up to six layers were included in the model: silicon substrate, native oxide, PDMS, LQG (or SCL, depending on the temperature), SG and another SCL layer (from bottom to top). Parameters for silicon, native oxide and PDMS at any temperature were used as described above. At each isothermal temperature, the Cauchy parameters for the LQG (or SCL) and SG were held constant based on previously measured values. Only the thicknesses of the LQG, SCL layer(s) and SG layers were allowed to vary as fitting parameters over time. Due to the substantial refractive index contrast between SG and LQG (or SCL), fixing the thickness of either the top or bottom evolving layer resulted in a large mean square error (Extended Data Fig. 8). As such, the temporal evolution of the interfaces' positions could be precisely determined.

We note that during isothermal annealing at $T_{iso} < T_g$, aging in the LQG layer is expected to slightly increase its refractive index with time. However, allowing this index to vary as a free parameter did not affect the overall results, as they did not substantially affect the measured thickness values (Extended Data Fig. 9). Consequently, the refractive index of this layer was held constant, and only the thickness was fitted to prevent overfitting.

Calculation of $\Delta\rho$, T_f and birefringence

The relative density change, $\Delta\rho$, is determined from the average refractive indices ($\langle n \rangle$) measured before and after the thermal transformation

of SG and bilayer films, using the Lorentz–Lorenz equation[42]. For optically anisotropic films ($n_{xy} \neq n_z$), $\langle n \rangle$ can be calculated as

$$\langle n \rangle = \sqrt{\frac{n_x^2 + n_y^2 + n_z^2}{3}} = \sqrt{\frac{2n_{xy}^2 + n_z^2}{3}}. \quad (4)$$

The density of glass is correlated with its transparent refractive index through the Lorentz–Lorenz equation[42]:

$$\frac{n^2 - 1}{n^2 + 2} = \frac{\alpha N_A \rho}{3\epsilon_0 M_W}, \quad (5)$$

where ρ is the density, α is the molecular polarizability, N_A is the Avogadro number, ϵ_0 is the permittivity of free space and M_W is the molecular molar mass. This equation indicates that n can be used as an independent measure of density without relying on the thickness change on film transformation. Our previous work[43] has demonstrated that this correlation holds for TPD glass films over a broad range of film thicknesses.

Assuming the changes in n and ρ are small, we have

$$\frac{6n}{(n^2 + 2)^2} dn = \frac{\alpha N_A}{3\epsilon_0 M_W} d\rho. \quad (6)$$

By dividing equation (6) by equation (5), we get the relative changes:

$$\frac{d\rho}{\rho} = \frac{6n^2}{(n^2 + 2)(n^2 - 1)} \frac{dn}{n}. \quad (7)$$

We define $\Delta\rho = (\rho - \rho_{LQG})/\rho$ and $\Delta n = (n - n_{LQG})/n$ to substitute for $d\rho/\rho$ and dn/n, respectively; then, we have

$$\Delta\rho = \frac{6n^2}{(n^2 + 2)(n^2 - 1)} \Delta n. \quad (8)$$

With equation (8), the relative density change ($\Delta\rho$) can be calculated using the relative change in the refractive index (Δn), compared with the values of LQG at 298 K. For birefringent samples, $\langle n \rangle$ is used instead of n.

The fictive temperature, T_f, is calculated based on the temperature dependence of $\Delta\rho$ for equilibrium SCL and SG[29]. Birefringence is defined as the difference between the out-of-plane (n_z) and in-plane (n_{xy}) refractive indices. A lower birefringence, indicated by a smaller absolute value, signifies a more isotropic molecular orientation in the glass.

Estimation of average aging rate

Since the T_g value of 50-nm-thick LQG layers on both soft and rigid substrates are the same as bulk T_g (Extended Data Fig. 1a,b), their aging rates are expected to be similar to bulk samples. Furthermore, previous studies on polymer glasses have shown that the formation of a polymer/rubber interface does not affect the aging rate, even when the local T_g is substantially shifted[44,45]. Therefore, the average rate of change of the LQG layer thickness due to aging ($\langle v_{ag} \rangle$) was estimated based on the aging studies in ref. 33 in bulk TPD LQGs (Extended Data Fig. 3a,b). For simplicity, it was assumed that the aging rate is constant over the experimental time window. Although aging is not necessarily linear with time, $\langle v_{ag} \rangle$ was found to be much slower than $\langle dz_b/dt \rangle$ for most data points. As shown in Extended Data Fig. 3c, including $\langle v_{ag} \rangle$ in the calculation made no substantial difference, as $\langle dz_b/dt \rangle$ is nearly identical to the estimated value of $\langle v_{gr,b} \rangle$, confirming that the rate of aging had a negligible effect on the calculation of growth front velocity.

Data availability

The data that support the findings of this study are included in Extended Data Table 1. Source data are also available via figshare at https://doi.org/10.6084/m9.figshare.33014207.

References

42. Böttcher, C. J. F. & Bordewijk, P. *Theory of Electric Polarization, Vol. 2: Dielectrics in Time-Dependent Fields* (Elsevier, 1978).
43. Jin, Y. et al. Glasses denser than the supercooled liquid. *Proc. Natl Acad. Sci. USA* **118**, e2100738118 (2021).
44. McGuire, J. A., Merrill, J. H., Couturier, A. A., Thees, M. F. & Roth, C. B. Comparison of physical aging and glass transition in glassy–rubbery polymer bilayer films. *J. Phys. Chem. B* **129**, 2778–2788 (2025).
45. Rauscher, P. M., Pye, J. E., Baglay, R. R. & Roth, C. B. Effect of adjacent rubbery layers on the physical aging of glassy polymers. *Macromolecules* **46**, 9806–9817 (2013).

Acknowledgements

We thank L. M. C. Beltran for professional scientific editing and graphical assistance.

Author contributions

P.L. and Z.F. conceived the study, P.L. performed the experiments and analysed the data with the help of Z.L., Y.C., K.J., S.E.W., S.G., J.I.B.-L. and R.B.S. P.L. and Z.F. wrote the paper.

Funding

We acknowledge financial support from the Wisconsin Materials Research Science and Engineering Center (MRSEC) funded by National Science Foundation (NSF) grant number DMR-2309000. P.L. acknowledges postdoctoral fellowship funding from the School of Arts and Sciences of the University of Pennsylvania.

Competing interests

The authors declare no competing interests.

Additional information

Extended data is available for this paper at https://doi.org/10.1038/s41567-026-03394-1.

Correspondence and requests for materials should be addressed to Peng Luo or Zahra Fakhraai.

Peer review information *Nature Physics* thanks the anonymous reviewers for their contribution to the peer review of this work.

Reprints and permissions information is available at www.nature.com/reprints.

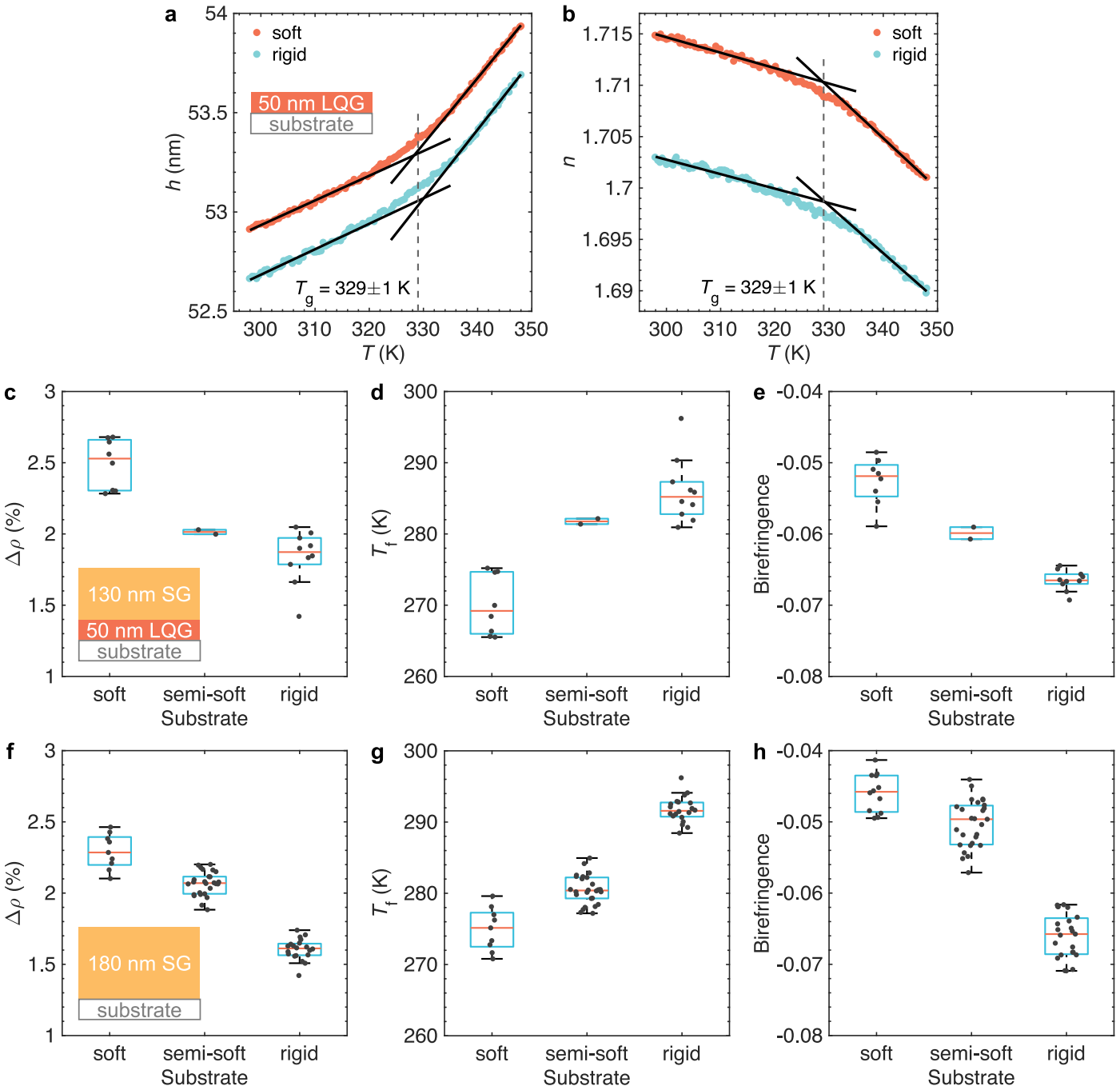
https://doi.org/10.1038/s41567-026-03394-1

Extended Data Table 1 | Transformation kinetics of SG(130 nm)/LQG(50 nm) bilayer films on rigid and soft substrates

T (K)	$\langle dz_b/dt \rangle$ on rigid substrate (nm/s)	$\langle dz_b/dt \rangle$ on soft substrate (nm/s)	$\langle v_{ag} \rangle$ (nm/s)	$\langle v_{gr,b} \rangle$ on rigid substrate (nm/s)	$\langle v_{gr,b} \rangle$ on soft substrate (nm/s)
348	1.9×10^{-1}	-	-	1.9×10^{-1}	-
343	$(2.2 \pm 0.2) \times 10^{-2}$	$(5.0 \pm 0.2) \times 10^{-2}$	-	$(2.2 \pm 0.2) \times 10^{-2}$	$(5.0 \pm 0.2) \times 10^{-2}$
338	2.3×10^{-3}	-	-	2.3×10^{-3}	-
333	1.7×10^{-4}	5.1×10^{-4}	1.4×10^{-7}	1.7×10^{-4}	5.1×10^{-4}
328	3.8×10^{-6}	3.9×10^{-5}	2.2×10^{-7}	4.0×10^{-6}	3.9×10^{-5}
323	-	$(5.2 \pm 0.9) \times 10^{-6}$	2.8×10^{-7}	-	$(5.5 \pm 0.9) \times 10^{-6}$
318	-	2.3×10^{-7}	4.8×10^{-7}	-	7.1×10^{-7}

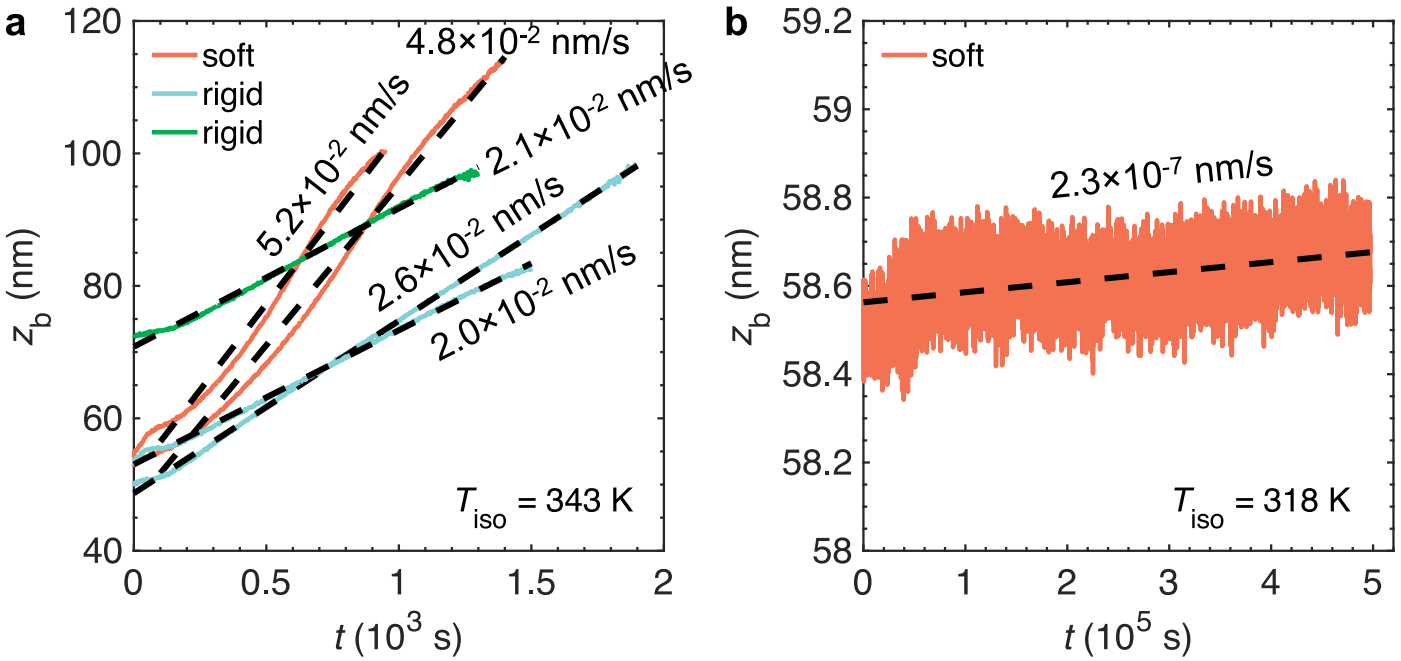
Measured values of $\langle dz_b/dt \rangle$ for the bilayer, the estimated aging velocity $\langle v_{ag} \rangle$ of the 50-nm LQG layer, and $\langle v_{gr,b} \rangle$ of the bilayer at various temperatures on rigid and soft substrates. Data with error bars are presented as mean values ± standard error of the mean for three independent experiments.

https://doi.org/10.1038/s41567-026-03394-1



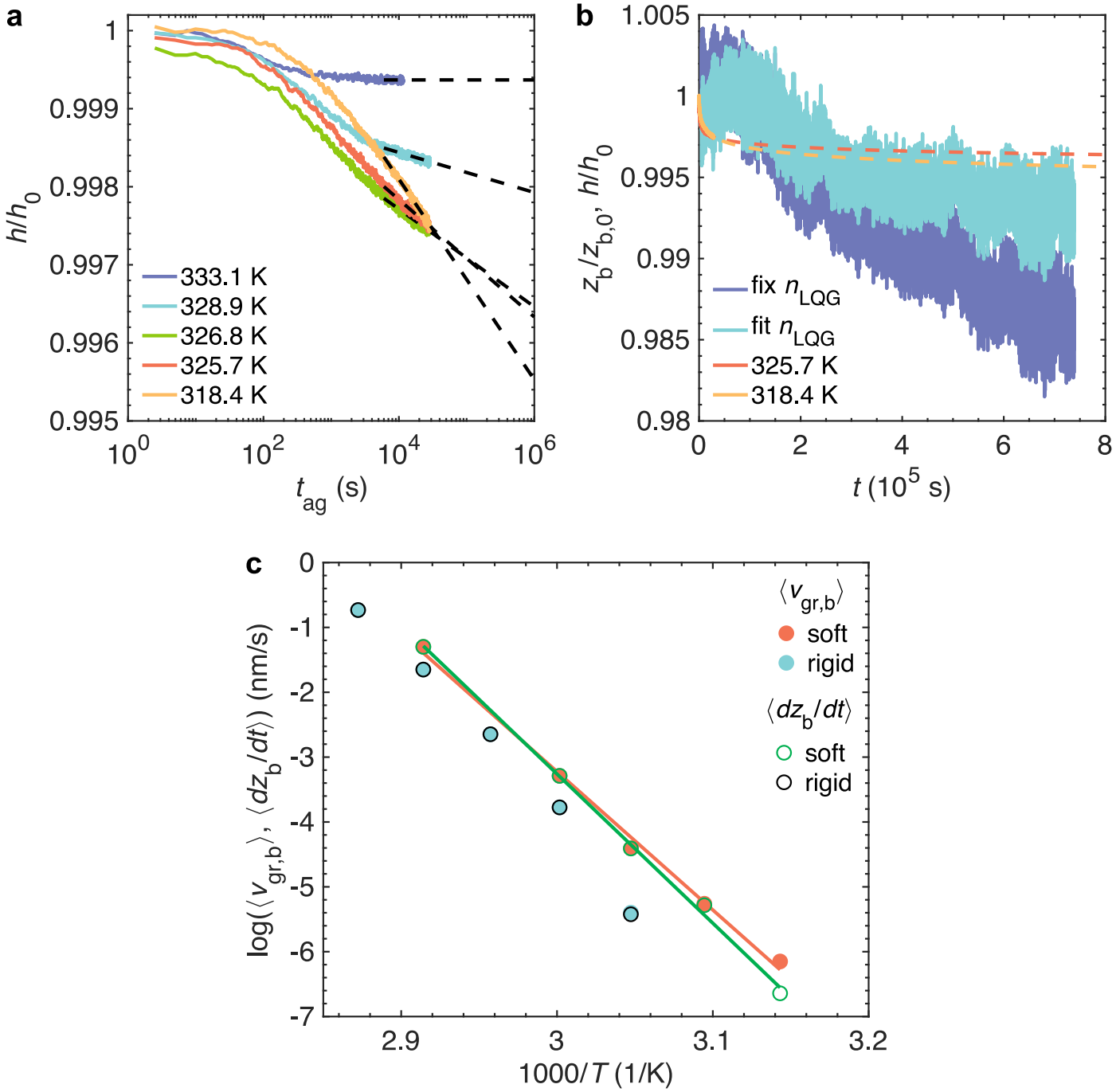
Extended Data Fig. 1 | Properties of the LQG and SG layers in bilayer and single-layer samples prepared on substrates of different elasticity. a,**b**, Thickness (**a**) and refractive index at $\lambda = 632.8$ nm (**b**) of 50-nm LQG films on soft and rigid substrates, as a function of temperature during cooling at 10 K/min. The glass transition temperature, T_g, is 329 ± 1 K on both types of substrates. **c**,**f**, Relative density change ($\Delta\rho$), **d**,**g**, fictive temperature (T_f), and **e**,**h**, birefringence of bilayer films comprising 130-nm-thick SG layers deposited on top of 50-nm-thick LQG layers (**c**-**e**) and single-layer 180-nm-thick SG films (**f**-**h**). For the box plots in **c**-**h**: center line is the median; box limits are at 25th and 75th percentiles; whiskers show the most extreme data points within 1.5 × interquartile range; and black data points are individual measurements. For bilayer SG films (**c**-**e**), the number of independent measurements was $N = 8$, 2, and 10, on soft, semisoft, and rigid substrates, respectively. For single-layer films (**f**-**h**), the corresponding numbers were $N = 12$, 27, and 23, respectively.

https://doi.org/10.1038/s41567-026-03394-1



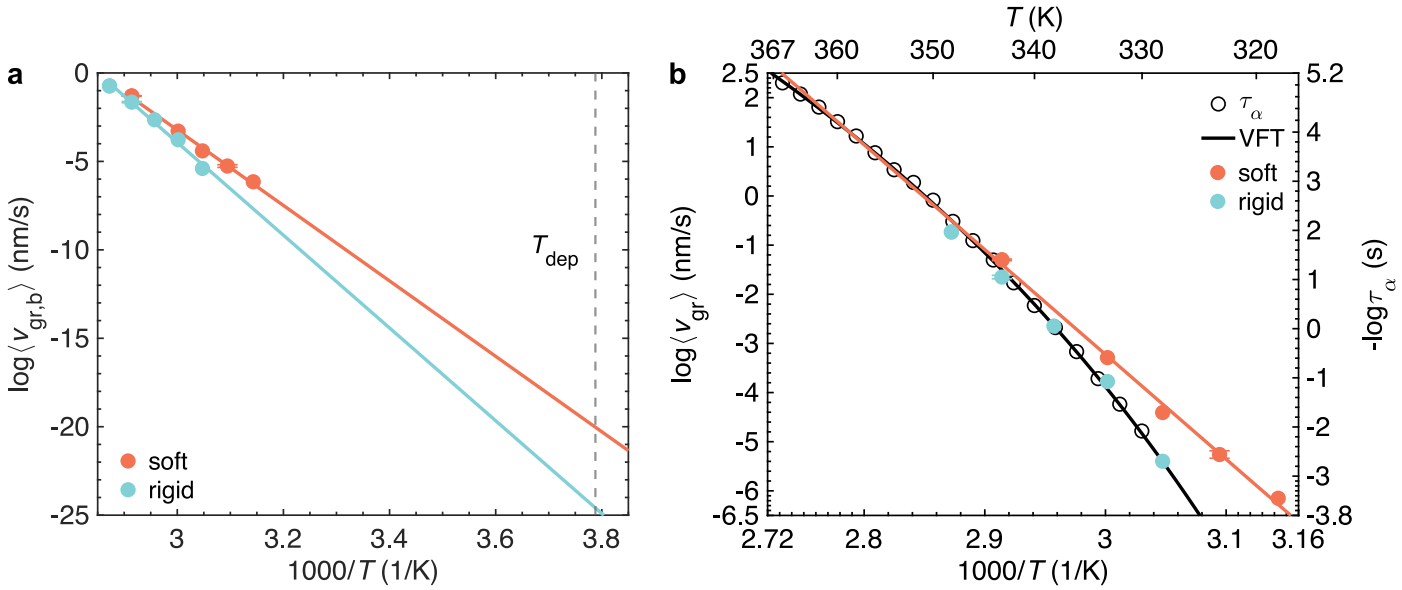
Extended Data Fig. 2 | z_b versus time during isothermal annealing at T_{iso} = 343 and 318 K. a, Independent transformation experiments at T_{iso} = 343 K (1.04T_g) were carried out on SG(130 nm)/LQG(50 nm) bilayers prepared on rigid (turquoise) and soft (red) substrates, and on a SG(110 nm)/LQG(70 nm) bilayer prepared on a rigid substrate (green). **b**, Transformation at T_{iso} = 318 K (0.97T_g) for a SG(130 nm)/LQG(50 nm) bilayer prepared on a soft substrate. For both **a** and **b**, dashed lines show the linear least-squares fits used to determine $\langle dz_b/dt \rangle$, defined as the fitted regression slope. The corresponding slope values are labeled beside each line. For **b**, the standard error of the fitted slope is 3.3×10^{-9} nm/s.

https://doi.org/10.1038/s41567-026-03394-1



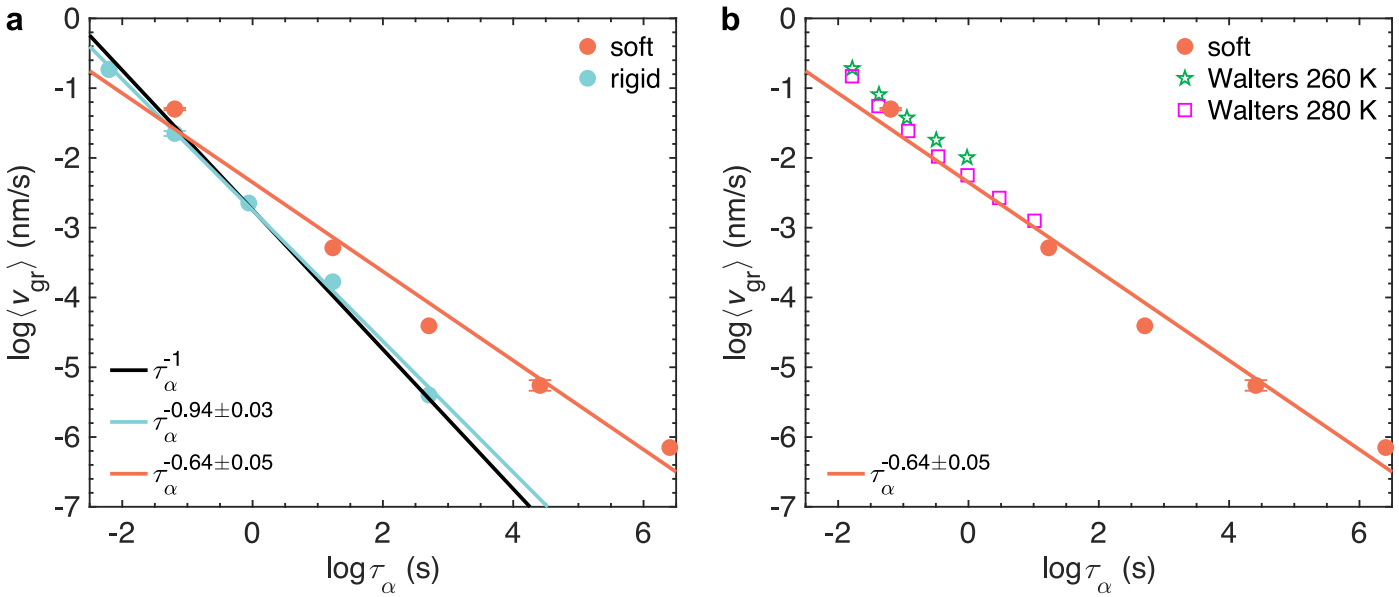
Extended Data Fig. 3 | Estimated aging of the 50-nm LQG layer and comparison of $\langle v_{gr,b}\rangle$ and $\langle dz_b/dt\rangle$ at the buried SG/LQG interface in bilayer films. **a**, Normalized thickness of 400-nm-thick LQG films as a function of aging time at various temperatures. Dashed lines show linear extrapolation on the log(t_{ag}) scale through the time window of the present experiments. **b**, Normalized position of the buried SG/LQG interface, $z_b/z_{b,0}$, as a function of time during isothermal annealing at T_{iso} = 323 K for a SG(130 nm)/LQG(50 nm) bilayer film prepared on a rigid substrate. The two datasets correspond to results obtained from two fitting approaches applied to the in situ SE data: one with the refractive index of the bottom LQG layer (n_{LQG}) fixed (blue-violet), and the other with n_{LQG} treated as a fitting parameter (turquoise). For comparison, the normalized thicknesses, h/h_0, of 400-nm-thick LQG films aged at 325.7 and 318.4 K, along with the extrapolated lines shown in **a**, are also plotted. $z_{b,0}$ and h_0 denote the corresponding values at t = 0 s. **c**, Arrhenius plot of $\langle v_{gr,b}\rangle$ and $\langle dz_b/dt\rangle$ for bilayer films. Solid lines are linear fits to $\langle v_{gr,b}\rangle$ and $\langle dz_b/dt\rangle$ for samples on soft substrates, yielding activation energies of 408 ± 15 kJ/mol (red) and 440 ± 12 kJ/mol (green), respectively. Aging data in panels **a** and **b** adapted with permission from ref. 33, Royal Society of Chemistry.

https://doi.org/10.1038/s41567-026-03394-1



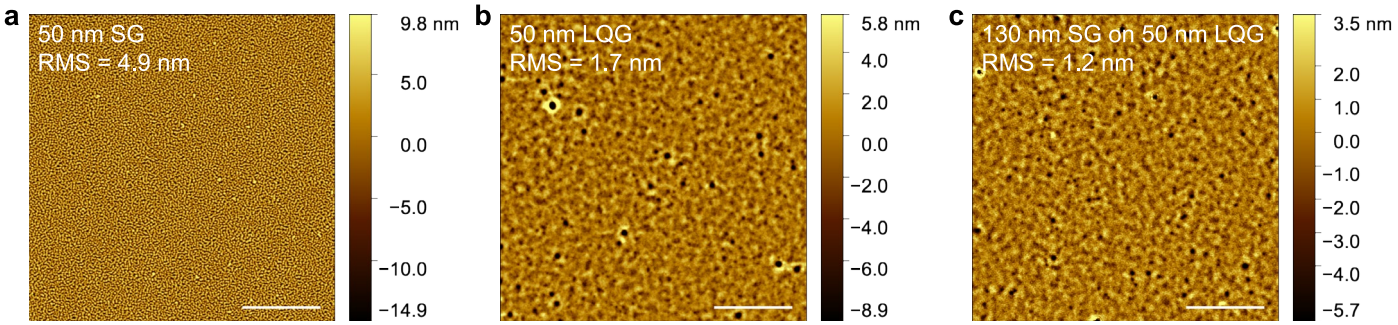
Extended Data Fig. 4 | Extrapolation of $\langle v_{gr,b} \rangle$ assuming Arrhenius temperature dependence. a, Extrapolation of $\langle v_{gr,b} \rangle$ to lower temperatures for bilayer films on soft and rigid substrates. The gray dashed line marks $T_{dep} = 264$ K. The corresponding activation energies are 408 ± 15 kJ/mol for the soft-substrate film and 502 ± 30 kJ/mol for the rigid-substrate film. **b**, Extrapolation of $\langle v_{gr,b} \rangle$ to higher temperatures for the bilayers on the soft substrate, shown as the solid red line. The measured $\langle v_{gr,b} \rangle$ (left axis) for the soft- (red) and rigid-substrate (turquoise) samples are compared with the bulk τ_α of TPD (right axis; black circles) and its VFT fit (black line), plotted as a function of inverse temperature ($1000/T$; corresponding temperature values are shown on top). Data with error bars are presented as mean values ± standard error of the mean for three independent experiments. τ_α data in panel **b** adapted with permission from ref. 30, AIP.

https://doi.org/10.1038/s41567-026-03394-1



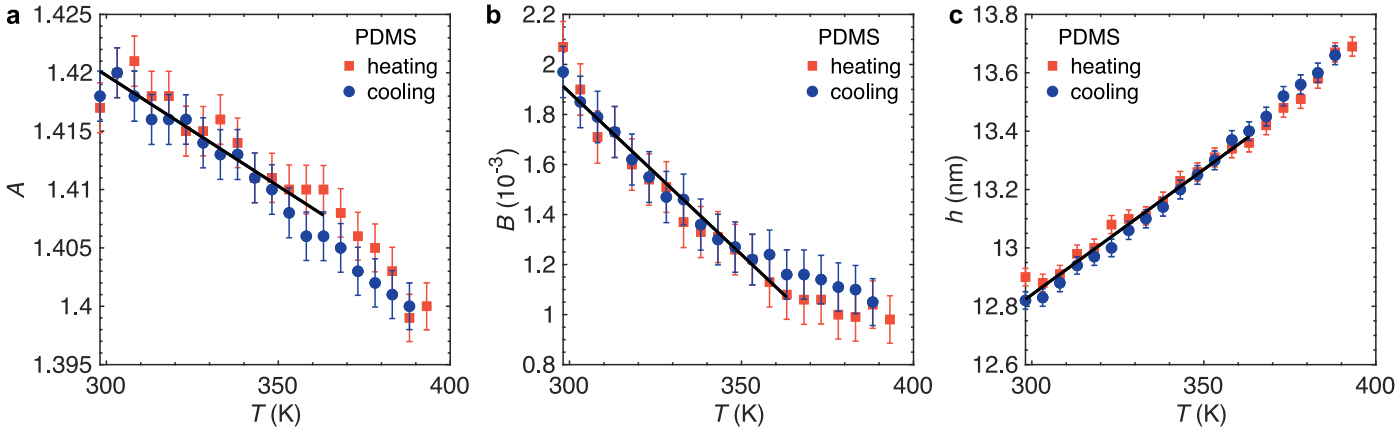
Extended Data Fig. 5 | Transformation front velocities as a function of the liquid structural relaxation time at the annealing temperature. a, $\log\langle v_{gr,b}\rangle$ for bilayer films on soft (red) and rigid (turquoise) substrates versus the structural relaxation times ($\log\tau_\alpha$) based on bulk TPD studies in ref. 30. **b**, $\log\langle v_{gr,b}\rangle$ for bilayers on soft substrates (red circles) versus $\log\tau_\alpha$ as well as the surface-initiated transformation front velocities reported by Walter et al.[30] for TPD SGs deposited at T_{dep} = 260 K (green stars) and 280 K (magenta squares). Data with error bars are presented as mean values ± standard error of the mean for three independent experiments. The colored lines are linear least-squares fits to the corresponding data points with the same color. The power-law exponents and uncertainties shown in the legends are the fitted regression slopes and their standard errors, respectively. The black line in **a** is a constrained fit to the data for the rigid substrate, with the slope fixed at −1. τ_α data in panel **a** and surface-initiated transformation data in panel **b** adapted with permission from ref. 30, AIP.

https://doi.org/10.1038/s41567-026-03394-1



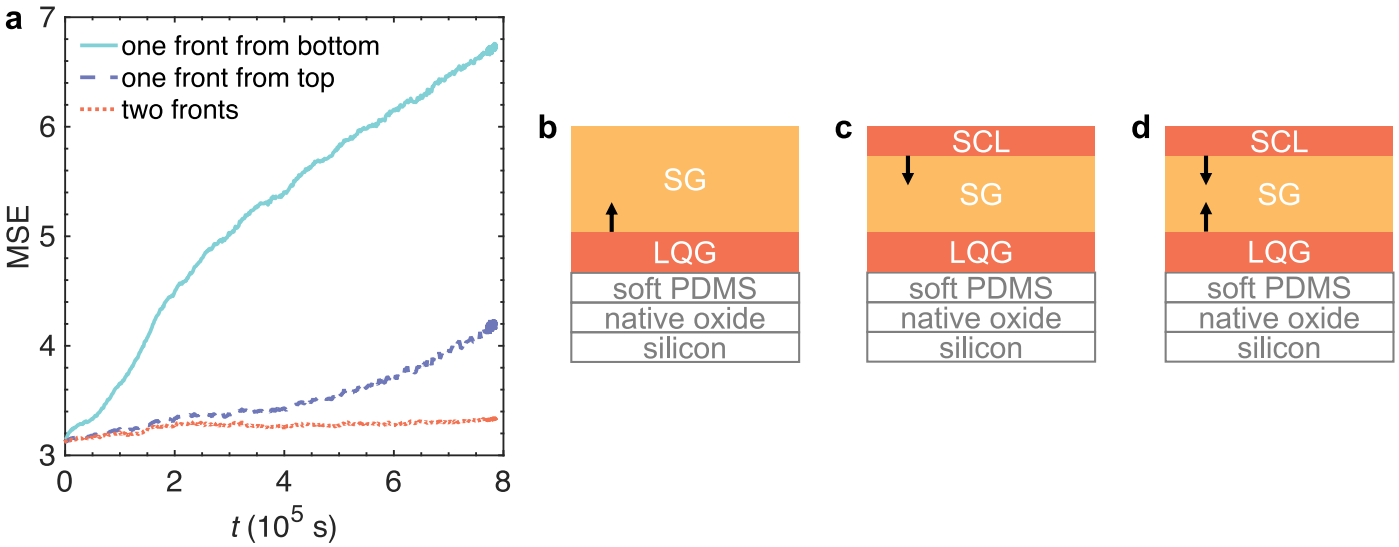
Extended Data Fig. 6 | Atomic force microscope (AFM) images of TPD glass films deposited on soft substrates. a, As-deposited 50-nm-thick SG film. **b**, LQG obtained by heating the SG film in **a** to the SCL state at 343 K for 10 min and quenching back to room temperature. **c**, A 130-nm-thick SG film deposited on a 50-nm-thick LQG layer. The scale bars for all images are 5 μm. Root-mean-square (RMS) roughness values are indicated on each image.

https://doi.org/10.1038/s41567-026-03394-1



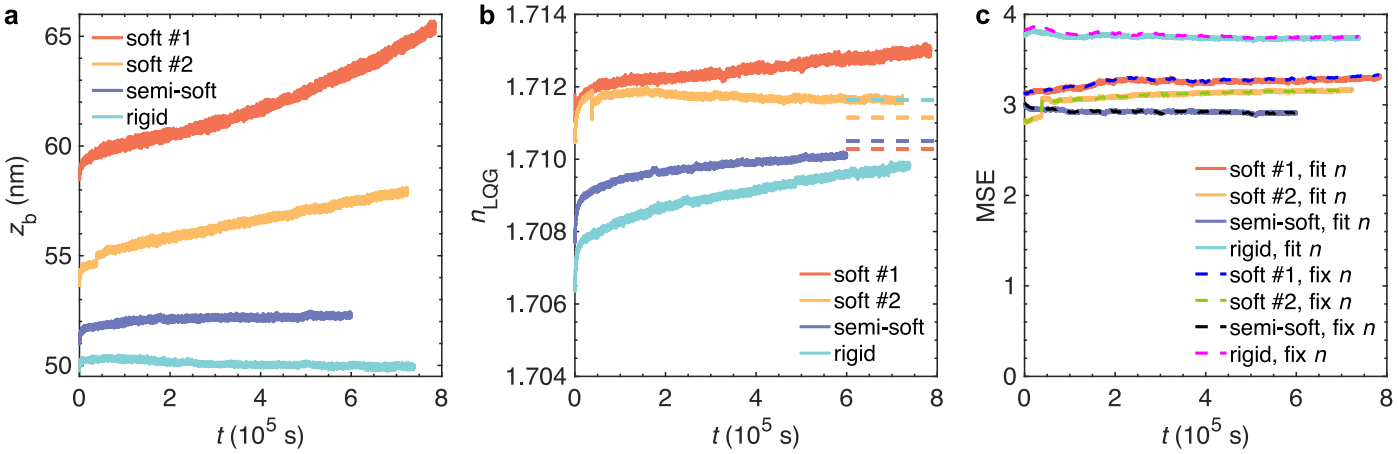
Extended Data Fig. 7 | Cauchy parameters of a 13-nm-thick PDMS film obtained by modeling the VASE data collected at various isothermal temperatures. Red squares represent the data obtained during heating from 298 to 393 K at 10 K/min, and with a 5-min isothermal hold at every 5-K interval. Blue circles are the data obtained upon subsequent cooling at the same rate, temperatures, and hold time. The results are presented as fitted values, with error bars indicating the 90% confidence intervals calculated using the CompleteEASE software's fitting algorithm. Solid lines are a global linear fit to both data sets in the temperature range between 298 and 363 K: **a**, $A = 1.4767 - 1.8967 \times 10^{-4} T$; **b**, $B = 5.7808 \times 10^{-3} - 1.2974 \times 10^{-5} T$; and **c**, $h = 10.2658 + 8.5802 \times 10^{-3} T$, with thickness h in nm and temperature T in K.

https://doi.org/10.1038/s41567-026-03394-1



Extended Data Fig. 8 | Comparing the mean square error (MSE) of various fitting models to the in situ spectroscopic ellipsometry (SE) data. a, MSE versus time during isothermal annealing of a modeled SG (130 nm)/LQG (50 nm) bilayer on a soft substrate at T_{iso} = 323 K. **b**–**d**, Schematic illustrations of the models used for fitting: **b**, one transformation growth front initiating from the SG/LQG interface (buried interface, corresponding to 'bottom' in **a**); **c**, one transformation growth front initiating from the free surface ('top' in **a**); and **d**, two transformation growth fronts initiating from the buried interface and the free surface, respectively. As seen in **a**, the model with two growth fronts (red) produces lower MSE than the other two models throughout the annealing experiment.

https://doi.org/10.1038/s41567-026-03394-1



Extended Data Fig. 9 | Modeling of the in situ spectroscopic ellipsometry (SE) data for the SG (130 nm)/LQG (50 nm) bilayer with the refractive index of the bottom LQG layer, n_{LQG}, as a fit parameter. a, z_b, **b**, n_{LQG}, and **c**, MSE, versus time during isothermal annealing at T_{iso} = 323 K, for bilayer samples on various substrates. Dashed lines in **b** indicate the n_{LQG} values of 180-nm-thick LQG films after full transformation of the bilayer and subsequent quenching to 323 K, following the same color scheme as the solid lines. Dashed lines in **c** correspond to the MSE of fittings with n_{LQG} fixed at the values as indicated by the dashed lines in **b**. The two independent trials on soft substrates were labeled as #1 and #2.